Critical Stress Analysis of Large Aircraft on Airport Rigid Pavement Using FEAFAA

Yuanguo Chen[1], Qiang Wang[2] and David R. Brill[3]

Abstract

The critical stresses of large aircraft on the airport rigid pavement were analyzed using 3D finite element program, FEAFAA. Four large aircraft with multiple-gear structures, the A380, B747, A340-500, and A340-200, were selected for the analysis. The curling effect on top-down cracking prediction was investigated through the equivalent temperature gradient (ETG). Among the curling directions of downward curling, flat and upward curling, the upward curling shows the greatest critical top-to-bottom tensile stress ratio (t/b ratio), as expected. Also, for upward curling, the t/b ratio shows a high linear dependence on the ETG value for the considered ETG range. The critical gear position is identified for upward curling: a critical gear position exists for A340-500 and A340-200, and a critical gear area exists for B747 and A380. Finally, the sensitivity analysis for the A380 shows that: the t/b ratio is highly sensitive to the slab thickness and the elastic modulus of the subgrade, but insensitive to the elastic modulus of the slab, subbase thickness, and the elastic modulus of the subbase; the t/b ratio tends to increase as the elastic modulus of the subgrade and slab thickness increase; and the critical gear position can be regarded insensitive to the elastic modulus and thickness of each pavement layer, since it is always located in the critical gear area.

Introduction

Aircraft manufacturers are designing aircraft with extended range capability. The high gross weight and new gear configuration result in the changes of pavement responses. To study the effects of high wheel loads with multiple gear configurations on the airport pavement is important for the improvement of pavement design procedure.

The Federal Aviation Administration (FAA) has based its airport rigid pavement thickness design procedure on the critical tensile stress. Traditionally, the critical tensile stress has been obtained using the Westergaard edge loading model (*FAA 1978*, *1995a*) which dates back to the 1920s (*Westergaard 1926*). With the emergence of new large aircraft such as the Boeing 777, the critical tensile stress was obtained using the layered elastic model, beginning with the LEDFAA 1.2 computer program (*FAA 1995b*).

At the same time, the finite element method (FEM) gradually gained acceptance for rigid pavement analysis (*GAO 1997*), and a 3D finite element program,

[1] *Yuanguo Chen, Ph.D., SRA International Inc., 1201 New Road, Suite #242, Linwood, NJ 08221, U.S.A., Phone: (609) 601-6800-151, Fax: (609) 601-6801, Email: yuanguo_chen@sra.com*

[2] *Qiang Wang, Ph.D., ISCP member, SRA International Inc., 1201 New Road, Suite #242, Linwood, NJ 08221, U.S.A.,Phone: (609) 601-6800-165, Fax: (609) 601-6801, Email: qiang_wang@sra.com*

[3] *David R. Brill, Ph.D., Federal Aviation Administration, Airport Technology R&D Team, U.S.A., Phone: (609) 485-5198; Fax: (609) 485-4845, Email: David.Brill@faa.gov*

Finite Element Analysis - FAA (FEAFAA), was developed for airport rigid pavement analysis (*Brill 1998*). A simplified version of this finite element model was used to compute the critical tensile stress in the FAA's new design procedure (*FAA 2009*).

The efforts so far on airport rigid pavement thickness design have focused mainly on the critical tensile stress at the bottom of a slab (i.e. critical bottom tensile stress), or the bottom-up cracking. However, the critical tensile stress at the top of a slab (i.e. critical top tensile stress) may exceed the critical bottom tensile stress and induce top-down cracking. For example, the full-scale tests at FAA's National Airport Pavement Test Facility (NAPTF), which aim to provide performance data for the FAA's new design procedure, indicated a large amount of top-down cracking. Similar top-down cracking has also been observed in highway rigid pavement (*Mahoney et al 1997*, *Smith et al 1996*).

Many factors have been studied to explain top-down cracking. For example, test results from Construction Cycle 2 at NAPTF suggested that load transfer across dowelled joints induces some top-down cracking (*Brill 2005*). Numerical calculations showed that the consideration of full aircraft, instead of only an individual gear, increases the likelihood of top-down cracking (*Evangelista and Roesler 2009*). Also, it has been suggested that the concrete strength at the top of the slab may be less than that at the bottom of slab (*McCullough and Dossey 1999*, *Fabre and Balay 2005*) which if true, would increase the likelihood of top-down cracking.

Another, and probably the most important, contributing factor is curling. For example, the corner top-down cracking in Construction Cycle 1 at NAPTF was found to be induced by the combined effect of mechanical load and curling (*Guo 2006*). The curling effect has long been studied. Westergaard (*Westergaard 1927*) pioneered this area through an analytical approach, and later the curling effect was incorporated in a 2D finite element model (*Lee and Darter 1994, Rufino et al 2004*). Improvements were recently made to FEAFAA to account for the curling effect (*Wang and Chen 2011*), with which the curling effect was investigated for airport rigid pavement subject to individual gear (*Khazanovich*, unpublished manuscript*, 2010*). Such investigation, however, has not been made for airport rigid pavement subject to multiple-gear aircraft.

Objectives

The objective of this study is to investigate the curling effect on top-down cracking prediction for airport rigid pavement subject to four multiple-gear aircraft: the A380, B747, A340-500, and A340-200. Critical top tensile stress is evaluated at different gear positions using the 3D finite element program FEAFAA. The critical gear position, critical top tensile stress position, and the critical top-to-bottom tensile stress ratio (t/b ratio) are identified under the curling condition. Sensitivity analysis is performed to investigate the effect of elastic modulus and thickness of each pavement layer.

Methodology

Finite Element Program FEAFAA. In this study, the finite element program FEAFAA is used to perform all calculations. FEAFAA uses NIKE3D (*Maker 1995*) and INGRID (*Christon and Dovey 1992*) as its computation engine and mesh engine respectively. NIKE3D is a general-purpose finite element code and INGRID is the accompanying mesh generator. Both were originally developed at Lawrence Livermore National Laboratory (LLNL) and extensively modified by the FAA to meet the requirements of rigid pavement analysis (*FAA 2010*).

Under many years of continuous development, FEAFAA has obtained the capability of modeling infinite elements, sliding contact surface, etc. In addition, FEAFAA uses spring elements to model the joints and the load transfer between adjacent slabs. Recent development includes a sliding interface model with self-adjustable scale factor and two types of curling shape: circular and catenary (*Wang and Chen 2011*). In this paper, only the circular curling is considered.

Pavement Structure. The baseline pavement structure is described in Table 1. The resilient modulus *E* of 66 MPa (9616 psi) of the subgrade is equivalent to the foundation modulus of the subgrade *k* = 27 MPa/m (100 pci), according to the conversion embedded in FAA's thickness design program FAAEFIELD ($E = 26\ k^{1.284}$ in US Unit). Similarly, a 15 cm (6 in) subbase P154 on a 27 MPa/m (100 pci) subgrade, FAARFIELD computes a modulus E = 116 MPa (16,848 psi) using the internal modulus subroutine. These values are used as a starting point. The bold values are varied in the sensitivity study discussed later in this paper.

For PCC slabs, a 3×3 slab system (Figure 1) is used. A uniform mesh is used for both the slab and foundation (subbase and subgrade). Each slab is divided into a 40 × 40 mesh. For the foundation elements, a coarse (50 × 50) mesh is used. By default FEAFAA uses one layer of elements along the slab thickness and five layers of elements along the foundation thickness. To compensate for the accuracy loss in the slab, the incompatible element mode is used for all elements excluding the infinite element. The mesh used in this paper is to balance the accuracy and computation time.

Table 1. Pavement Structure

	Elastic Modulus *E*	Poisson's ratio	Thickness h
PCC Slab	**31026** MPa (4,500,000 psi)	0.15	**41** cm (16 in)
Subbase (P154)	**116** MPa (16,848 psi)	0.2	**15** cm (6 in)
Subgrade	**66** MPa (9,616 psi)	0.4	-

Multiple-Gear Aircraft. Four multiple-gear aircraft are selected. These four aircraft have the different multiple gears: A380 has a gear of 2D/3D2, B747 of 2D/2D2, A340-500 of 2D/2D1, and A340-200 of 2D/D1. The basic gear information was extracted from FAARFIELD and then modified as needed in the external library of FEAFAA. Figure 2 provides a graphical view of the four aircraft. Note that the A340-500 and A340-200 have different tire pressure and contact area between their wind gear and body gear. They are simplified to assume the same tire pressure and contact area in this study. The actual gear configurations are listed in Table 2. For completeness, the simplifed gear configurations for the A340-500 and A350-200 are also listed.

Each selected aircraft has one plane of symmetry, so only half of the gear positions need to be especially considered. Symbol "•" in Figure 1 denotes a possible position of the gear's center of geometry (CG). Using a distance interval of 76 cm (30 in), a total of 66 gear positions (6×11) need to be considered. For illustrative convenience, Figure 1 also plots the wheel positions at the initial (#1) and final (#66) gear position for A380.

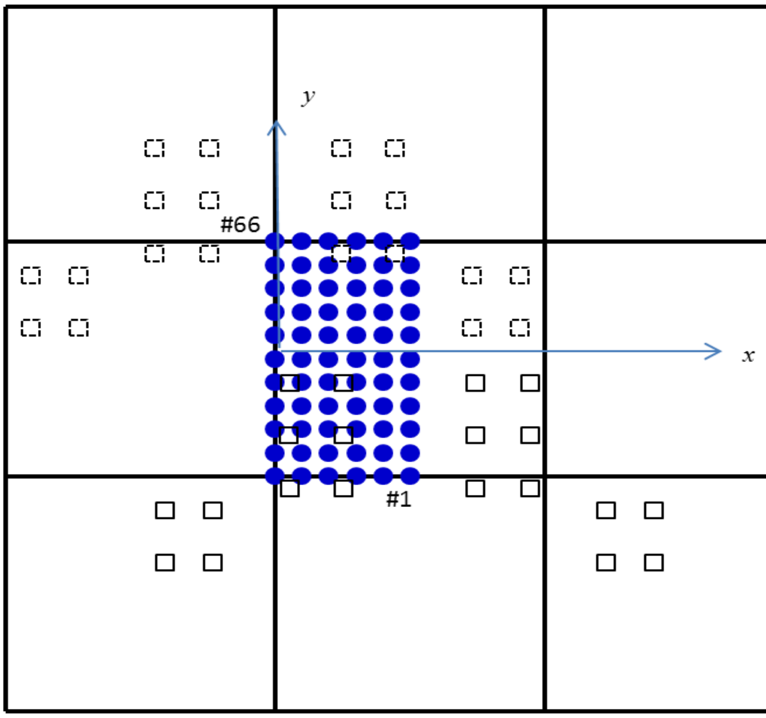

Figure 1. Slab configuration and gear positions (symbol "•"denotes a possible position of the gear's center of geometry (CG). The solid squares and dashed squares denote the wheel position of A380 at initial gear position #1 and final gear position #66, respectively).

Table 2. Main Gear Configuration

		Actual Gear		Simplified Gear	
		Wing Gear	Body Gear	Wing Gear	Body Gear
A380 (Gross Weight = 5,511kN)	Gear Load* (%)	38%	57%	N/A	N/A
	No. of Gears	2	2		
	Wheels on Each Gear	4	6		
	Tire Pressure (MPa)	1.38	1.38		
	Contact Area (cm^2)	1,898	1,898		
B747 (Gross Weight = 3,719 kN)	Gears Weight (%)	47.5%	47.5%	N/A	N/A
	No. of Gears	2	2		
	Wheels on Each Gear	4	4		
	Tire Pressure (MPa)	1.31	1.31		
	Contact Area (cm^2)	1,685	1,685		
A340-500 (Gross Weight = 3,621 kN)	Gears Weight (%)	66%	29%	63.3%	31.7%
	No. of Gears	2	1	2	1
	Wheels on Each Gear	4	4	4	4
	Tire Pressure (MPa)	1.61	1.53	1.59	1.59
	Contact Area (cm^2)	1,855	1,724	1,811	1,811
A340-200 (Gross Weight = 2,529 kN)	Gears Weight (%)	78%	17%	76%	19%
	No. of Gears	2	1	2	1
	Wheels on Each Gear	4	2	4	2
	Tire Pressure (MPa)	1.32	1.09	1.27	1.27
	Contact Area (cm^2)	1,869	1,973	1,894	1,894

* Assuming 95% of gross airplane weight on the main gear.

At each gear position (each "•"), the top and bottom tensile stresses are recorded for the slab system. The maxima of these maximum tensile stresses for all 66 gear positions are defined as the critical top and bottom tensile stresses respectively, and the corresponding gear position as the critical gear positions.

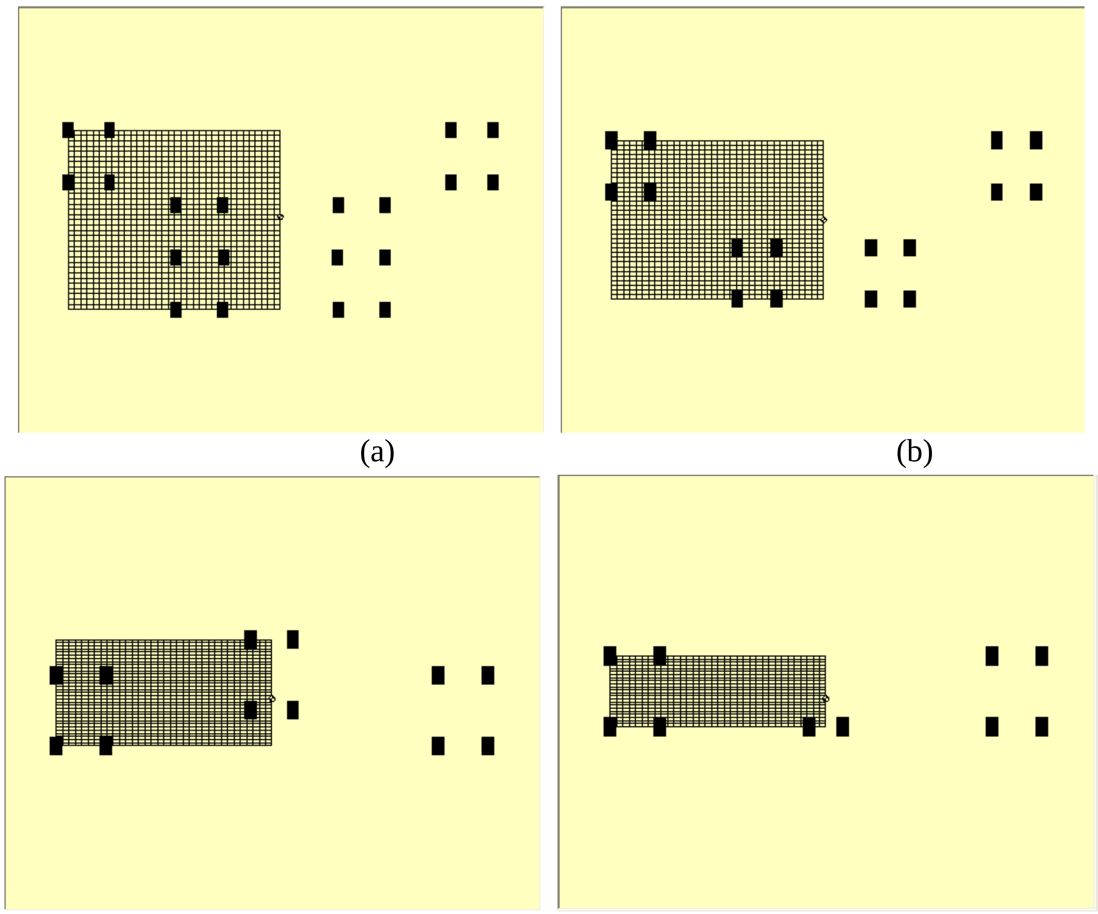

(a) (b) (c) (d)

Figure 2. Multiple-gear aircraft (A) A380, (B) B747, (C) A340-500 and (D) A340-200.

The t/b Ratio. FAA's design procedure uses design factor (DF) to predict airport rigid pavement performance. The DF is defined as

$$DF = \frac{R}{\sigma} \tag{1}$$

Where, R is the concrete flexural strength and σ the critical tensile stress.

Equation 1 does not indicate the direction of cracking and thus should apply to both bottom-up and top-down cracking. To predict which cracking pattern will appear first, Equation 1 can yield

$$\frac{DF(top)}{DF(btm)} = \frac{R(top)/R(btm)}{\sigma(top)/\sigma(btm)} \tag{2}$$

Where, "*top*" denotes events at the top of slab and "*btm*" the bottom. If $\sigma(top)/\sigma(btm) < R(top)/R(btm)$, then $DF(top) > DF(btm)$ and bottom-up cracking is expected to appear first. Otherwise top-down cracking appears first. This, of course, answers that cracking will first appear on the surface with the highest stress.

For any given slab, *R*(*top*)/*R*(*btm*) is assumed constant, so Equation 2 solely depends on $\sigma(top)/\sigma(btm)$, i.e. the critical top-to-bottom tensile stress ratio (t/b ratio). In other words, the t/b ratio can serve as the indicator of the cracking pattern: the higher the t/b ratio, the more likely that when cracking initiates, it will be top-down.

Result Analysis

Effect of Curling Direction on the t/b Ratio. A slab may curl upward or downward, depending on the on-site factors such as temperature, shrinkage, moisture, and curing, etc. The curling direction can be characterized through the equivalent temperature gradient (ETG): A slab curls downward at positive ETG, curls upward at negative ETG, and remains flat at zero ETG.

First observed is the effect of curling direction on the t/b ratio. Table 3 summarizes the tensile stresses at the top and bottom of slab and the t/b ratio. The curling direction of DOWNWARD, FLAT, and UPWARD corresponds to ETG value of 0.2734 °C/cm (1.25 °F/in), 0, and -0.2734 °C/cm (-1.25 °F/in), respectively.

Table 3. The Effect of Curling Direction on The t/b Ratio

	Curling Direction	Top (MPa)		Bottom (MPa)		t/b ratio
		σxx	σyy	σxx	σyy	
A380	DOWNWARD	**1.21**	0.96	4.01	**4.12**	0.29
	FLAT	**1.86**	1.45	2.81	**2.99**	0.62
	UPWARD	**2.99**	2.20	**2.48**	**2.48**	1.21
B747	DOWNWARD	**0.95**	0.89	3.72	**4.10**	0.23
	FLAT	1.45	**1.47**	2.45	**2.92**	0.50
	UPWARD	2.11	**2.30**	2.13	**2.57**	0.89
A340-500	DOWNWARD	**1.85**	1.20	4.09	**4.48**	0.41
	FLAT	**2.30**	1.72	2.92	**3.36**	0.68
	UPWARD	**2.97**	2.36	2.47	**2.99**	1.00
A340-200	DOWNWARD	**1.26**	0.83	3.66	**4.21**	0.30
	FLAT	**1.79**	1.39	2.45	**3.03**	0.59
	UPWARD	**2.63**	2.14	2.03	**2.56**	1.03

NOTE: Bold value is the critical tensile stress.

Figure 3 illustrates the variation of the t/b ratio with the curling direction under consideration. It is evident that the t/b ratio increases significiently from downward curling (positive ETG) to upward culing (negative ETG). In other words, top-down cracking is more likely to happen at negative ETG, as is well known. Therefore, the following analysis will concentrate on negative ETG only.

The calculations in this study are performed using FEAFAA. Evangelista and Roesler performed calculations for the flat slab system subject to several multiple-gear aircraft using the 2D finite element program ILLISLAB (*Roesler et al 2007*). The ILLISLAB study differed from the present study, since it used a Winkler foundation (i.e. characterized by the modulus of subgrade reaction) and had no ability to model curled slabs.

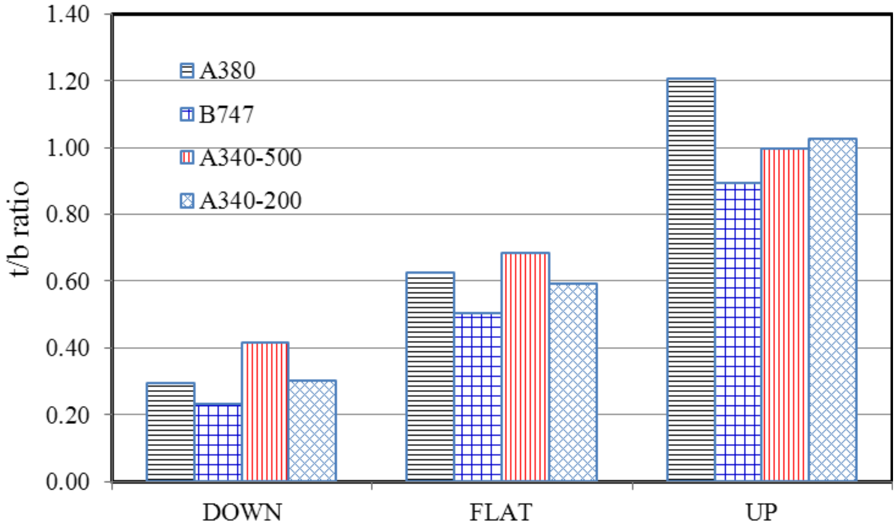

Figure 3. The variation of the t/b ratio with curling direction.

The results for FLAT in Table 3 are compared with results from Roesler et al. Table 4 summarizes the comparisons between FEAFAA and ILLISLAB. Because different tire pressures and contact areas, and consequently different gross weights, are used in the previous study, the results in Table 4 are the critical top tensile stress value divided by the gross weight. This eliminates the influence of load magnitude.

From Table 4 it can be observed that FEAFAA agrees fairly well with ILLISLAB with a load transfer efficiency (LTE) of 85%. The differences may be due to the different techniques used in modeling the load transfer: FEAFAA uses spring elements while ILLISLAB uses a single LTE. ILLISLAB with a LTE of 85% consistently computes a larger value than FEAFAA, a closer agreement is expected if a larger value of LTE is used.

Table 4. Comparison of FEAFAA with ILLISLAB

Aircraft	FEAFAA (MPa/kN)	ILLISLAB(MPa/kN)	
		LTE=85%	LTE=0%
A380	3.38E-04	4.45E-04	8.23E-04
B747	3.95E-04	4.42E-04	8.91E-04
A340-200[a]	7.08E-04	7.50E-04	1.32E-03

[a]MD-11 is used in previous study for gear 2D/D1

Effect of Negative ETG Value on t/b Ratio. To observe the effect of negative ETG value on the t/b ratio, three ETG values, i.e. 0, -0.1367 °C/cm (-0.625 °F/in), and -0.2734 °C/cm (-1.25 °F/in), are further studied.

Figure 4(a) illustrates the variation of the t/b ratio with negative ETG values. Compared to Figure 3, Figure 4(a) shows highly linear dependence of t/b ratio on the negative ETG value for the considered ETG range. Table 5 summarizes the linear regression equations between the t/b ratio and negative ETG value for each selected aircraft.

One must be reminded that the model in FEAFAA is nonlinear essentially and the stress at a specific point, in a general sense, should be nonlinear. However, as far as the critical stress is concerned, which is picked from all points on the slabs, it appears that the critical stress, and consequently the t/b ratio, behaves approximately linearly. Such linearity has also been found at cases with other large loadings and structure configurations: as we increased the wheel load values, the critical stress increased approximately proportionally, as shown in Figure 4(b) (*chen*, unpublished manuscript*, 2011*).

Figure 4(a) also shows that among the four aircraft the B747 exhibits the lowest t/b ratio. Of the four airplanes, only the A380 and A340-200 had a t/b ratio greater than 1.00 (at the maximum negative ETG), which could be interpreted as predicting a higher likelihood of top-down cracking occurring for those airplane loadings.

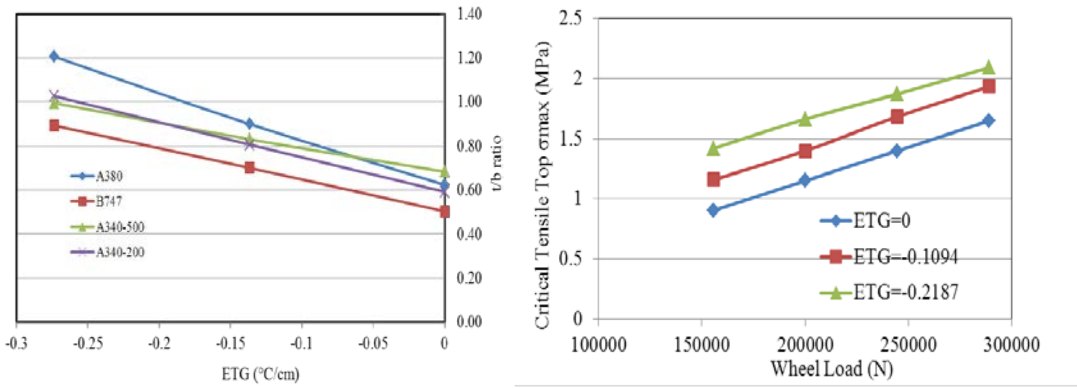

(a) (b)

Figure 4. The variation of (a) t/b ratio with ETG values, and (b) critical stress with wheel load values.

Table 5. Regression Equation between the t/b Ratio and Negative ETG Value.

Aircraft	Regression Equation	Coefficient of Determination (R^2)
A380	-2.1287ETG+0.6187	0.9992
B747	-1.4236ETG+0.5045	0.9999
A340-500	-1.1397ETG+0.6807	0.9988
A340-200	-1.5897ETG+0.5913	0.9999

Critical Gear Position. In this analysis, it is answered that the location of the critical top tensile stress corresponds to the slab location where top-down cracks are likely to initiate. Likewise, the accompanying gear position is the critical gear position for computing the top-down tensile stress.

For each aircraft, the critical gear position is identified through computational results. Some gear positions, although not the critical one, yield a maximum top tensile stress very close to the critical top tensile stress (no less than 97% of the critical top tensile stress). They are identified as alternative critical gear positions.

The critical gear position, alternative critical gear positions if applicable, and the corresponding maximum top tensile stress positions are plotted in Figures 5 through 9, where symbol "•" denotes the position of the gear's CG for the critical gear position and all alternative critical gear positions, and "×" the corresponding maximum top tensile stress positions. A dashed arrow "- -►" connects the gear position and the corresponding maximum top tensile stress position if alternative critical gear positions appear.

For each aircraft, Figures 5 through 9 also plot the wheel positions corresponding to the critical gear position (denoted by symbol "■") and, if applicable, one alternative critical gear position (denoted by symbol "□"). Their position numbers are marked with the number underlined corresponding to the critical gear position.

A380

Figure 5 illustrates the critical gear position, alternative critical gear positions, and their corresponding maximum top tensile stress positions for the A380. For flat slab (ETG=0), the critical gear position occurs at #31(229 cm, 229 cm) (90 in, 90 in). When -0.1367 °C/cm (-0.625 °F/in), the critical gear position shifts to #2(381 cm, -305 cm) (150 in, -120 in) and remains there when ETG = -0.2734 °C/cm (-1.25 °F/in).

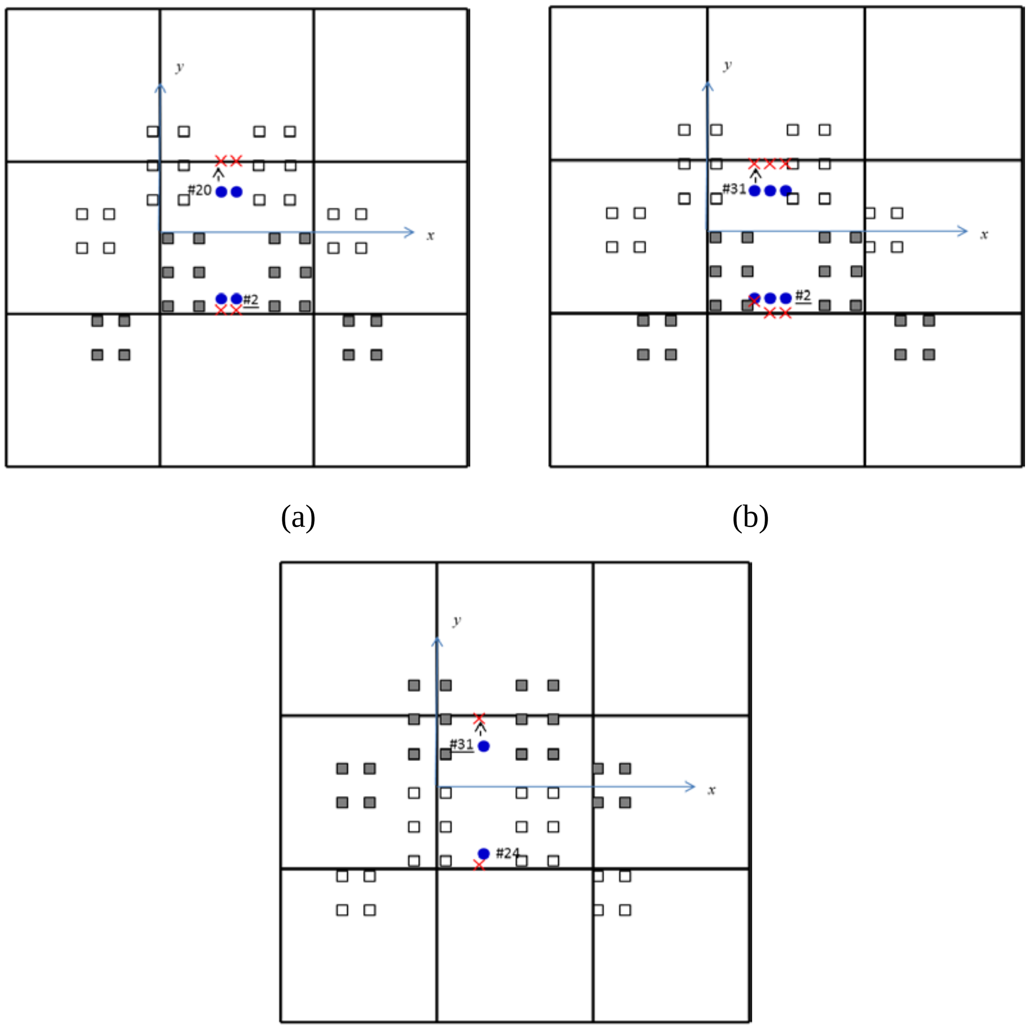

(a) (b)

(c)

Figure 5. Critical gear position for A380 at (a) ETG = -0.2734 °C/cm (-1.25 °F/in), (b) ETG = -0.1367 °C/cm (-0.625 °F/in), and (c) ETG = 0.

The critical gear position is not fixed for the three ETG values. If the alternative critical gear positions are considered, it appears that the (alternative) critical gear positions occur in the area that y_c =229 cm (90 in) and y_c = -305 cm (-120 in) in with x_c spanning from 229 cm (90 in) to 381 cm (150 in), where x_c and y_c are the *x*- and *y*-coordinate of CG hereafter. This area includes #2, #9, #13, #20, #24, and #31 and is identified as the critical gear area of A380.

Let x_f and y_f denote the *x*- and *y*-coordinate of the maximum top tensile stress position. For the (alternative) critical gear positions, it can be found that $x_f \approx x_c$, while

y_f≈381 cm (150 in) or -381 cm (-150 in). In other words, these maximum top tensile stresses are located on the slab transverse edge.

B747

Figure 6 illustrates the critical gear position, alternative critical gear position, and their corresponding maximum top tensile stress positions for the B747. For flat slab (ETG=0), the critical gear position occurs at #30(229 cm, 152 cm) (90 in, 60 in), and remains there when ETG = -0.1367 °C/cm (-0.625 °F/in). When ETG = -0.2734 °C/cm (-1.25 °F/in), the critical gear position shifts to #10(381 cm, 305 cm) (150 in, 120 in).

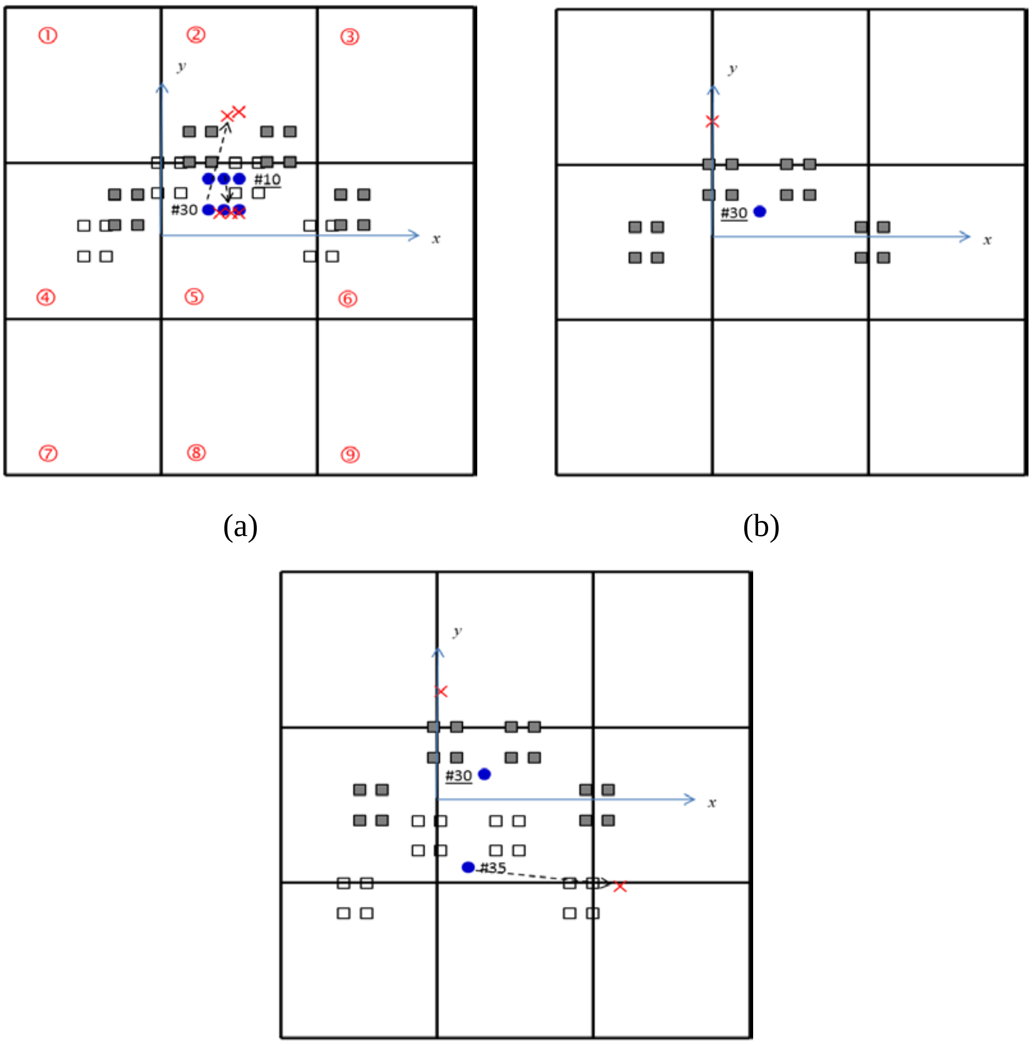

(a) (b) (c)

Figure 6. Critical gear position for B747 at (a) ETG = -0.2734 °C/cm (-1.25 °F/in), (b) ETG = -0.1367 °C/cm (-0.625 °F/in), and (c) ETG = 0.

The critical gear position is not fixed for the three ETG values. If the alternative critical gear positions are considered, it appears that the (alternative) critical gear positions occur in the area that y_c = 152 cm (60 in) or y_c = 305 cm (120 in) with x_c spanning from 229 cm (90 in) to 381 cm (150 in). This area includes #8, #10, #19, #21, #30, and #32 and is identified as the critical gear area of B747. Also, #30 can best serve as the critical gear position for the three ETG values: it is already the critical gear position when ETG=0 and ETG = -0.1367 °C/cm (-0.625 °F/in), and it is also the alternative critical gear position when ETG = -0.2734 °C/cm (-1.25 °F/in).

From Figure 6 it may be observed that the maximum top tensile occurs in the slab adjacent to the slab landed by the two body gears of the B747. For example, for gear position #10 in Figure 6(a) the body gears load slab② and the maximum top tensile stress is identified by the "×" on slab⑤. By contrast, when the body gears are positioned on slab⑤ (load case #30), the critical maximum tensile stress is on adjacent slab②.

A340-500

Figure 7 illustrates the critical gear position, alternative critical gear position, and their corresponding maximum top tensile stress positions for the A340-500. When ETG=0, the critical gear position occurs at #13(305 cm, -305 cm) (120 in, -120 in), and remains there when ETG = -0.1367 °C/cm (-0.625 °F/in) and ETG = -0.2734 °C/cm (-1.25 °F/in). So #13 is the critical gear position for the three ETG values. In such a gear position, the body gear (the middle 4 wheels) straddles the transverse joint (*x*-direction), and the right wind gear (the right 4 wheels) straddles the corner of adjacent slab.

The maximum top tensile stress occurs between the right wind gear and the body gear with $y_f \approx$ -381 cm (-150 in). With upward curling increasing, x_f slightly shifts toward the body gear.

A340-200

For the A340-200, the critical gear position occurs at #21(305 cm, 305 cm) (120 in, 120 in) for the three ETG values. In such a gear position, the body gear (the middle 2 wheels) straddles the transverse joint (*x*-direction), and the wind gear (the right 4 wheels) straddles the corner of adjacent slab.

Similar to the A340-500, the maximum top tensile stress occurs between the right wind gear and the body gear, but with $y_f \approx$ 381 cm (150 in). With upward curling increasing, x_f slightly shifts toward the body gear.

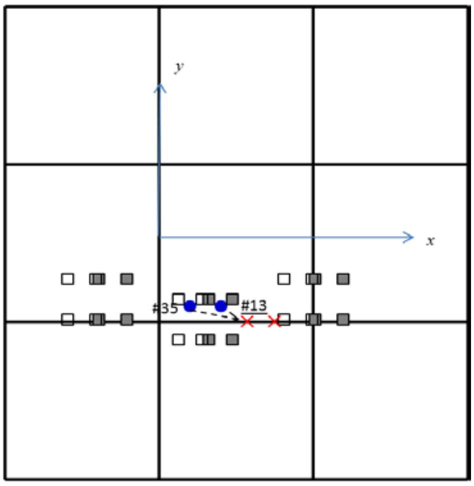

(a)

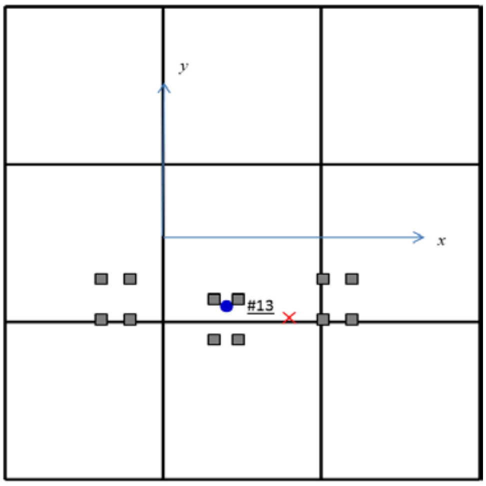

(b)

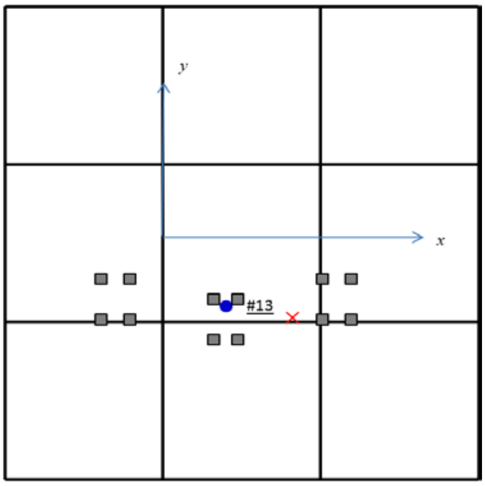

(c)

Figure 7. Critical gear position for A340-500 at (a) ETG = -0.2734 °C/cm (-1.25 °F/in), (b) ETG = -0.1367 °C/cm (-0.625 °F/in), and (c) ETG = 0.

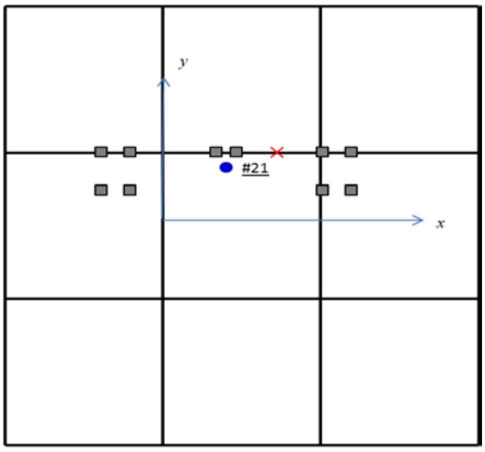

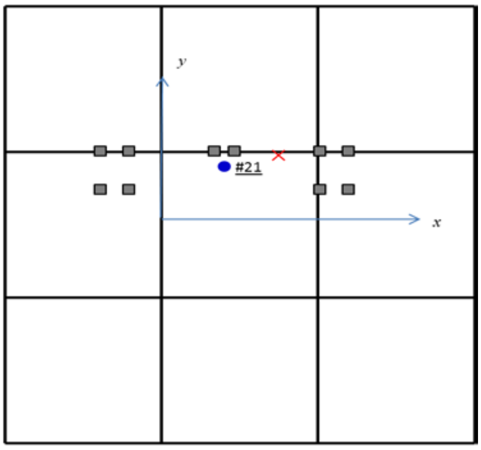

(a) (b)

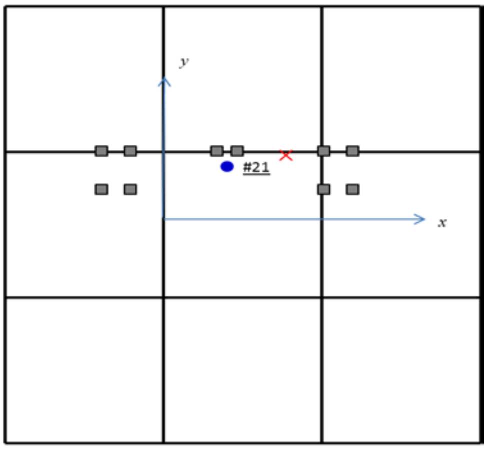

(c)

Figure 8. Critical gear position for A340-200 at (a) ETG = -0.2734 °C/cm (-1.25 °F/in), (b) ETG = -0.1367 °C/cm (-0.625 °F/in), and (c) ETG = 0.

Simplified Gear vs. Actual Gear. A simplified gear with uniform tire pressure, as presented in Table 2, is used for the A340-500 and A340-200. It is necessary to examine if such a simplification would alter the maximum tensile top stress position or value.

Several cases, including both ETG=0 and ETG=-0.2734 °C/cm (-1.25 °F/in), with actual gear configuration have been selected for comparsion with the simplified gear configuration. Figure 9 plots the comparisons of maximum top tensile stress position (Figure 9a) and stress value (Figure 9b). It is evident that the simplified gear does not alter significantly the maximum top tensile stress position nor the value.

Since the maximum top tensile stress is normally located at some distance from the tires themselves, the value is more influneced by the total gear load than by individul tire characteristics. The effect of varying tire pressure is thus of a secondary order, and the decision to simplify the analysis for the A340 such that all tires on the main gear have equal tire pressure is justified. It is also noted that, while the ratio of the wing gear load to the body gear load is different for the acutal and simplified gears (Table 2), the sum of the weights of the body gear and wing gear are much closer (63.3% for the actual gear versus 62% fo the simplified gear, expressed as a percentage of the gross airplane weight).

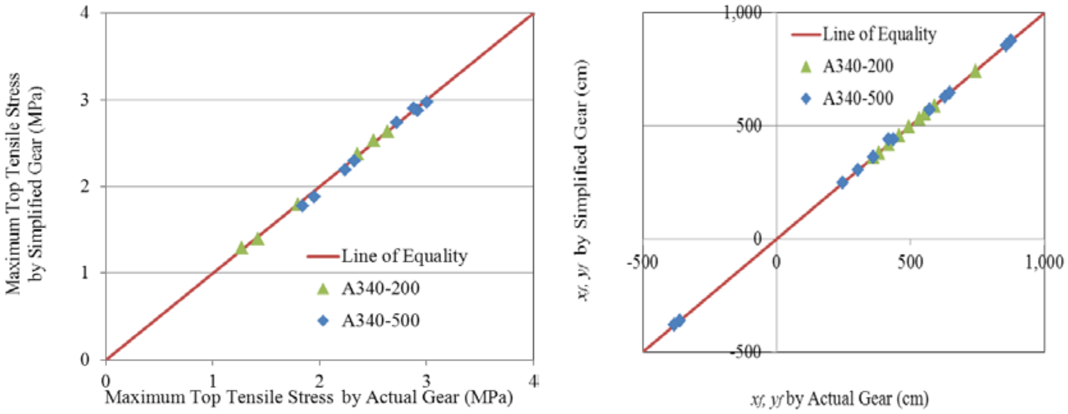

(a) (b)

Figure 9. The comparison of (a) maximum tensile top stress position, and (b) maximum tensile top stress value between actual gear and simplified gear for A340-500 and A340-200.

Sensitivity Analysis

Previous discussions have focused on the baseline structure given in Table 1. This section will investigate the sensitivity of the computed critical tensile stress and t/b ratio to variations in the elastic modulus and thickness of each pavement layer. For this purpose, the discussion is restricted to the A380 load with an assumed ETG=-0.2734 °C/cm (-1.25 °F/in).

Elastic Modulus of Subbase. The baseline pavement structure remains the same, except the subbase material P-154 E = 116 MPa (16848 psi) is changed to P-301 E = 1,724 MPa (250,000 psi) and P-306 E = 4,826 MPa (700,000 psi). Figure 10 plots the variation of the critical top and bottom tensile stresses and the t/b ratio with the elastic modulus of subbase.

Figure 10 shows that with the elastic modulus of the subbase increasing, the critical top and bottom tensile stresses tend to decrease, while the t/b ratio tends to increase. The variation is so insignificant that the critical top and bottom tensile stress and the t/b ratio can be regarded as insensitive to the elastic modulus of the subbase.

The critical gear position does not change and is always located at position #2.

Subbase Thickness. Figure 11 illustrates the variation of critical top and bottom tensile stress and the t/b ratio with subbase thickness of 15 cm (6 in), 25 cm (10 in) and 36 cm (14 in). With subbase thickness increasing, the critical top tensile stress tends to decrease while the critical bottom tensile stress to increase. As a result t/b ratio tends to decrease with the subbase thickness increasing. However, the variation is insignificant. Practically, the critical top and bottom tensile stress and the t/b ratio can be also regarded as insensitive to the subbase thickness.

The critical gear position does not change and is still located at position #2.

From Figures 10 and 11 and the observation of unchanged critical gear position, it can be concluded that the curling effect is insensitive to the subbase layer.

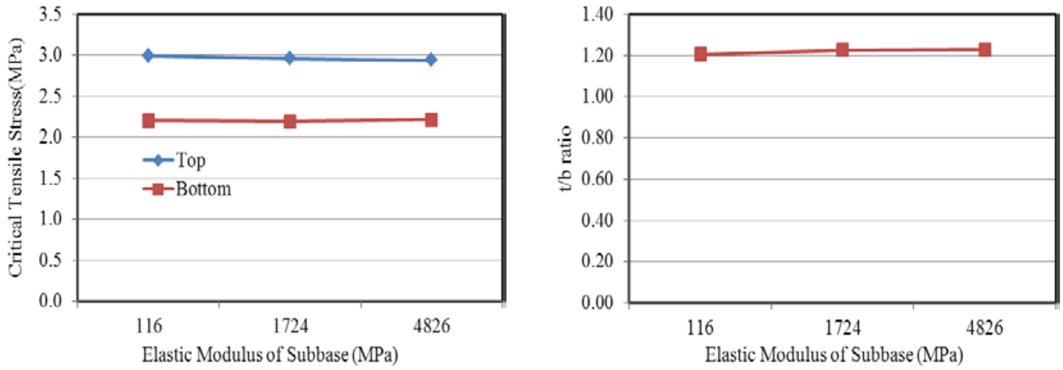

(a) (b)

Figure 10. The variation of (a) critical tensile stress, and (b) t/b ratio with elastic modulus of the subbase.

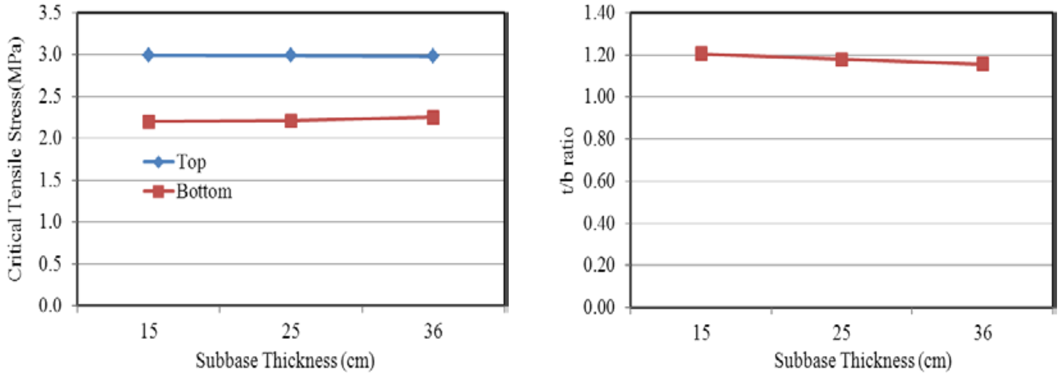

(a) (b)

Figure 11. The variation of (a) critical tensile stress, and (b) t/b ratio with subbase thickness.

Elastic Modulus of Subgrade. The elastic modulus of the subgrade in the baseline pavement structure is 66 MPa (9,616 psi). This elastic modulus is here changed to 112 MPa (16,184 psi) and 161 MPa (23,451 psi) (equivalent to changing the *k*-value from 100 pci to 200 pci). Since P-154 is still used for the subbase, the elastic modulus of the subbase is changed to 180 MPa (26,134 psi) and 217 MPa (31,523 psi) accordingly. Again, these values reflect those that would be computed automatically by the FAARFIELD program.

Figure 12 plots the variation of the critical top and bottom tensile stresses and the t/b ratio with the elastic modulus of the subgrade: As the elastic modulus of the subgrade increases, the critical top tensile stress barely changes, while the critical bottom tensile stress decreases and the t/b ratio increases appreciably.

With the elastic modulus of subgrade increasing, the critical gear position shifts to #9. In spite of this, this gear position is still located in the same general area identified in Figure 5.

Comparing Figure 12 with Figures 10 and 11, the critical bottom tensile stress and the t/b ratio are both more sensitive to the subgrade than to the subbase. The critical top tensile stress is insensitive to both the subgrade and the subbase. The t/b ratio increases as the subgrade stiffness increase (larger elastic modulus).

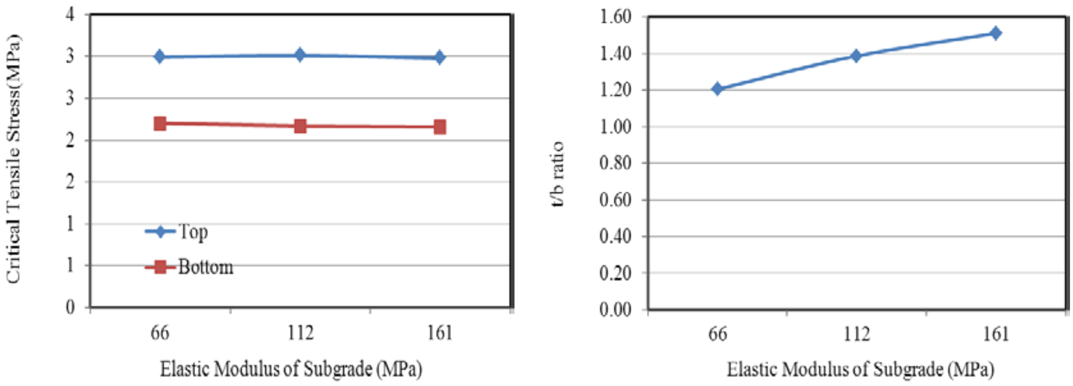

(a) (b)

Figure 12. The variation of (a) critical tensile stress, and (b) t/b ratio with elastic modulus of subgrade.

Elastic Modulus of Slab. The elastic modulus of the slab is 31,026 MPa (4,500,000 psi) in the baseline structure. Varying the elastic modulus in the range 24,132 MPa (3,500,000 psi) to 37,921 MPa (5,500,000 psi) has the effect as shown in Figure 13.

With the elastic modulus of slab increasing, the critical top and bottom tensile stresses increase concurringly. The critical top tensile stress increases at a slightly higher rate than its counterpart, and thus the t/b ratio increases slightly when the elastic modulus of slab increases. But the variation is not very strong and can be treated as constant, for design purposes. In other words, the t/b ratio can be regarded as practically insensitive to the elastic modulus of the slab.

The critical gear position remains at #2 with the elastic modulus of slab increasing but shifts to #9 with the elastic modulus of slab decreasing. Again, both #2 and #9 belong in the critical area identified in Figure 5.

Slab Thickness. The slab thickness was varied in the range 15 cm to 41 cm (6 to 16 inches) to identify the effect of thinner PCC slabs. Figure 14 illustrates the variation of critical top and bottom tensile stresses and the t/b ratio with slab thickness. The critical top and bottom tensile stresses decrease as slab thickness increases. The critical bottom tensile stress, however, decreases much faster than its counterpart, and as a result the t/b ratio increases with the slab thickness increasing.

The critical gear position shifts to #20 as the slab thickness decreases, which is still located in the critical gear area.

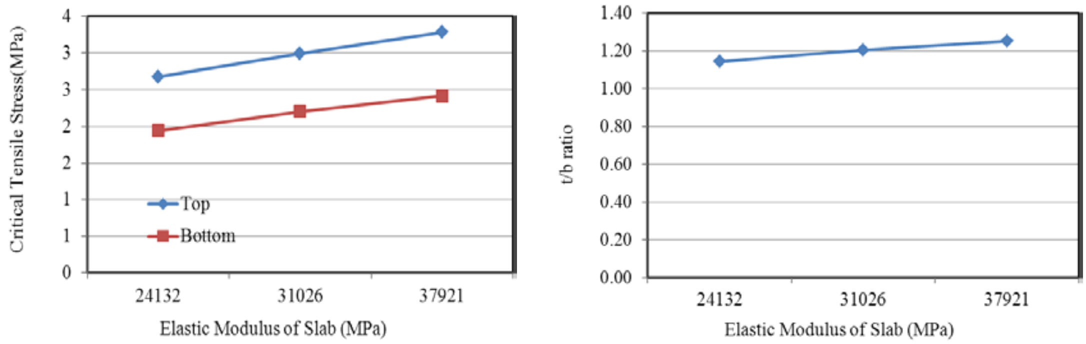

(a) (b)

Figure 13. The variation of (a) critical tensile stress, and (b) t/b ratio with elastic modulus of slab.

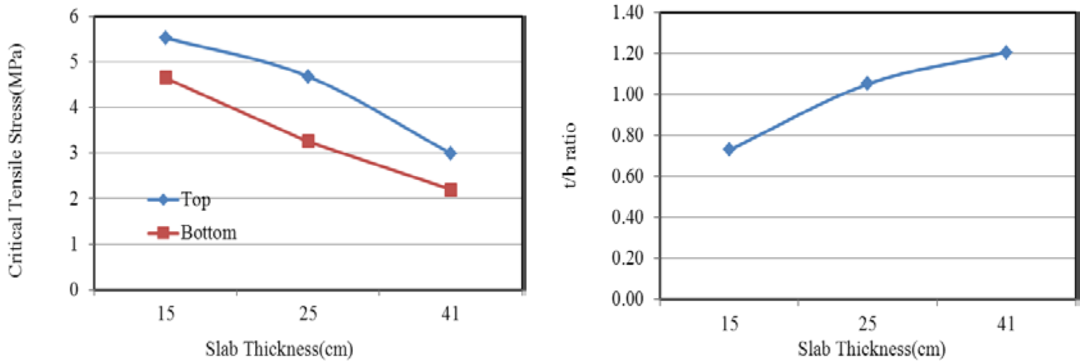

(a) (b)

Figure 14. The variation of (a) critical tensile stress, and (b) t/b ratio with slab thickness.

Figures 10 through 14 show that the t/b ratio is highly sensitive to the slab thickness and the elastic modulus of subgrade, but insensitive to the elastic modulus of the slab, subbase thickness, and elastic modulus of thes subbase. Also, the t/b ratio tends to increase as the elastic modulus of the subgrade and slab thickness increase.

Although the critical gear position may shift, it is always located in the critical gear area. In this sense, the critical gear position can be regarded as not very sensitive to the elastic modulus and thickness of the supporting pavement layers.

Conclusions

The objective of this study was to investigate the curling effect on top-down cracking prediction for airport rigid pavement subject to four multiple-gear aircraft: the A380, B747, A340-500, and A340-200. The 3D finite element program FEAFAA was employed which characterizes the curling through the equivalent temperature gradient (ETG).

Among three possible curling directions, i.e. downward curling, flat, and upward curling, the upward curling shows the greatest t/b ratio, as expected. Also, for upward curling, the t/b ratio shows a highly linear dependence on the ETG value.

The critical gear position is identified for upward curling: a critical gear position exists for A340-500 and A340-200, and a critical gear area exists for B747 and A380.

Finally, a sensitivity analysis was performed for the A380. The t/b ratio is highly sensitive to the slab thickness and the elastic modulus of the subgrade, but insensitive to the elastic modulus of the slab, subbase thickness, and the elastic modulus of the subbase. Also, the t/b ratio tends to increase as the elastic modulus of the subgrade and slab thickness increase. The critical gear position can be regarded as insensitive to the elastic modulus and thickness of each pavement layer, since its position is always located in the critical gear area.

Acknowledgments
The FAA Airport Technology R&D Branch, Dr. Satish K. Agrawal, Manager, supported the work described in this paper. The contents of the paper reflect the views of the authors, who are responsible for the facts and accuracy of the data presented within. The contents do not necessarily reflect the official views and policies of the FAA. The paper does not constitute a standard, specification, or regulation. Acknowledgment is given to Jeffrey Gagnon, and Dr. Gordon Hayhoe of the FAA Airport Technology R&D Branch, and to Chuck Teubert, Jerry Connelly, and Dr. Izydor Kawa of SRA International Inc.

References

Brill, D. R. (1998). *Development of advanced computational models for airport pavement design*, Report No. DOT/FAA/AR-97/47.

Brill, D. R., G. H. Hayhoe, and Ricalde, L. (2005). "Analysis of CC2 Rigid Pavement Test Data from the FAA's National Airport Pavement Test Facility". *7th International Confernce on the Bearing Capacity of Road, Railways, and Airfields* (CD-Rom), Trondhein, Norway.

Christon, M. A., and Dovey, D. (1992). *INGRID-A 3D mesh generator for modeling nonlinear systems*, UCRL-MA-109790 (Draft), Lawrence Livermore National Laboratory, Livermore, CA.

Evangelista Junior, F., and Roesler, J. R. (2009). "Top-Down Cracking Predictions for Airfield Rigid Pavements". *Transportation Research Record: Journal of the Transportation Research Board*, No. 2095, 13-23.

FAA. (1978). *Airport Pavement Design and Evaluation,* Advisory Circular 150/5320-6C, Federal Aviation Administration.

FAA. (1995a). *Airport Pavement Design and Evaluation,* Advisory Circular 150/5320-6D, Federal Aviation Administration.

FAA. (1995b). *Airport Pavement Design for the Boeing 777 Airplane,* Advisory Circular 150/5320-16, Federal Aviation Administration.

FAA. (2009). *Airport Pavement Design and Evaluation,* Advisory Circular 150/5320-6E, Federal Aviation Administration.

FAA. (2010). *FAARFIELD 1.305*, Federal Aviation Administration. <http://www.airporttech.tc.faa.gov/naptf/download/index1.asp> (July 06, 2011).

Fabre, M. C. and Balay, J. M. (2005). "A380 Pavement Experimental Programme, Rigid Tests". In *FAA Pavement Workgroup Meeting* (CD-Rom), NJ.

GAO. (1997). *Transportation Iinfrastructure: highway pavement design guide is outdated*, RCED-98-9, Government Accountability Office, D.C.

Guo, E. H. (2006). "Fundamental Modeling of Curling Responses in Concrete Pavements". In *6th International Workshop on Fundamental Modeling of Design and Performance of Concrete Pavements* (CD-Rom), Belgium.

Lee, Y. H., and Darter, M. I. (1994). "Loading and Curling Stress Models for Concrete Pavement Design", *Transportation Research Record: Journal of the Transportation Research Board*, No. 1449, 101-113.

Mahoney, J., J. A. Lary, L. M. Pierce, N. C. Jackson, and Barenberg, E. J. (1991). *Urban interstate Portland cement concrete pavement rehabilitation alternatives for Washington State.* Report No. WA-RD 202.1, Washington State Department of Transportation, Seattle, WA.

Maker, B. M. (1995). *NIKE3D-A nonlinear, implicit, three-dimensional finite element code for solid and structural mechanics-user's manual report.* UCRL-MA-105268, Rev. 1, Lawrence Livermore National Laboratory, Livermore, CA.

McCullough, B. F., and Dossey, T. (1999). "Considerations for High-Performance Conrete Paving; Recommendations from 20 Years of Field Experience in Texas". *Transportation Research Record, Journal of the Transportation Research Board*, No. 1684, 17-24.

Roesler, J. R., Evangelista Junior, F., and Domingues, M. (2007). "Effect of Gear Positions on Airfield Rigid Pavement Critical Stress Locations". In *FAA Worldwide Airport Technology Transfer Conference* (CD-Rom), NJ.

Rufino, D., Roesler, J., and Barenberg, E. (2004). *Mechanistic analysis of pavement responses from Denver International Airport*, COE Report No. 26, FAA Center of Excellence for Airport Technology.

Smith, K. D., M. J. Wade, D. G. Peshkin, L. Khazabovich, H. T. Yu, and Darter M. I. (1996). *Performance of concrete pavements, Volume II-Evaluation of in-service concrete pavements*. Report No. FHWA-RD-95-110, Washington, DC.

Wang, Q. and Chen, Y.G. (2011). "Improvements to Modeling of Concrete Slab Curling by Using NIKE3D Finite Element Program". *Transportation Research Record*, *Journal of Transportation Research Board*, No. 2226, 71-81**.**

Westergaard, H. M. (1926). "Stresses in Concrete Pavements Computed by Theoretical Analysis", *Public Roads*, Vol. 7, No. 2, 25-35.

Westergaard, H. M. (1927). "Analysis of Stresses in Concrete Roads Caused by Varaitions of Temperature", *Public Roads*, Vol. 8, No. 3, 54-60.